

The Indian Monsoon Circulation Response to El Niño Diabatic Heating

YOUKYOUNG JANG

Center for Ocean–Land–Atmosphere Studies, Calverton, Maryland

DAVID M. STRAUS

Department of Atmospheric, Oceanic, and Earth Sciences, George Mason University, Fairfax, and Center for Ocean–Land–Atmosphere Studies, Calverton, Maryland

(Manuscript received 31 October 2011, in final form 23 April 2012)

ABSTRACT

The response of the boreal summer mean tropical circulation to anomalies in diabatic heating during the strong El Niño events of 1972, 1987, and 1997 is studied, with particular focus on the Indian region. In experiments with the atmospheric general circulation model of the National Center for Atmospheric Research, anomalous diabatic heating fields are added to the full temperature tendency of the Community Atmosphere Model, version 3 (CAM3). The boundary conditions are specified climatological sea surface temperatures everywhere but over the Indian and western Pacific Oceans, where a slab-ocean model is used. The vertical structure of the added heating is idealized with a single maximum at 600 hPa. The added heating in the experiments was chosen on the basis of the 1972, 1987, and 1997 diabatic heating anomalies in the Pacific and Indian Oceans diagnosed from reanalyses. Integrations extended from May to August with 20 different initial conditions. The 1972 and 1987 experiments produced an anomalous anticyclonic circulation extending westward toward the Indian region, accompanied by negative total (added plus CAM3 produced) diabatic heating anomalies over India. A similar result was obtained for 1997 when only the Pacific Ocean diabatic heating was added. The heating over the central Pacific is shown to be more important than the western Pacific cooling. When the added heating also took into account anomalies over the Indian Ocean, the anomalous anticyclonic circulation weakens, while the total Indian heating anomaly is quite small. These results suggest the importance of the Indian Ocean heating for the 1997 monsoon circulation, but do not constitute a complete explanation since the Indian Ocean heating was given a priori.

1. Introduction

The El Niño–Southern Oscillation (ENSO) phenomenon is known to exert the single most important external forcing for the Indian summer monsoon (ISM) rainfall (Kumar et al. 1999; Lau and Nath 2000; Wang et al. 2003). The configuration of anomalously high pressure over the western Pacific–eastern Indian Ocean, and anomalously low pressure over the eastern/central Pacific associated with a El Niño event changes the tropical circulation significantly (Kumar et al. 1999; Palmer et al. 1992). In particular, ENSO changes both the rotational and divergent components of the seasonal mean flow; the accompanying changes in the vertical motion field affect

rainfall over the Indian region. This anomalous circulation mediates a negative relationship between eastern Pacific sea surface temperature (SST) associated with ENSO and the ISM. This relationship has led to ENSO being used as an important predictor in the statistical seasonal prediction of the Indian summer monsoon by Shukla and Paolino (1983) and Sahai et al. (2003). However, in recent years ENSO has seemingly lost its impact on the Indian summer monsoon (Kumar et al. 1999; Kripalani and Kulkarni 1997; Kirtman and Shukla 2000). For example, the strong El Niño in 1997 was accompanied by a normal monsoon, not a drought as expected.

In this paper, we focus on the monsoon circulation rather than the monsoon rainfall. Such an emphasis is motivated by the work of Straus and Krishnamurthy (2007), who found a higher interannual correlation between atmospheric circulation and ENSO-related SST than that between ISM rainfall and SST. The purpose of this study is to understand the ENSO–monsoon

Corresponding author address: Youkyoung Jang, Center for Ocean–Land–Atmosphere Studies, 4041 Powder Mill Rd., Suite 302, Calverton, MD 20705.
E-mail: yjang@cola.iges.org

relationship in terms of the rotational and divergent components and accompanying vertical motion, and also to focus on the circulation response to ENSO induced diabatic anomalies. Past studies of the ENSO–monsoon relationship have generally followed one of two approaches. In one approach, anomalous tropical SST is used as a boundary forcing (Charney and Shukla 1981) in a full atmosphere general circulation model (GCM; Wang et al. 2000; Lau and Nath 2000; Ju and Slingo 1995). Ashok et al. (2004), Kucharski et al. (2007), and Su et al. (2001) distinguished the atmosphere GCM response to the SST pattern in the 1997 event from the response to SST patterns for past El Niños, which were associated with a dry monsoon. However, in a full atmospheric GCM, the diabatic heating in the tropics may not respond realistically to the prescribed SST anomalies. Evidence for this is the generally poor mean monsoon simulation in many atmospheric GCMs (Palmer et al. 1992; Wu and Kirtman 2005). This difficulty is presumably related to the properties of the convective parameterization. A second approach has been to use an idealized atmospheric GCM (AGCM) with specified diabatic heating as the forcing (Lin 2009; Jin and Hoskins 1995). In this method, one has complete control over the diabatic heating, but cannot include any feedbacks associated with secondary convective responses to the forced circulation.

We use anomalous diabatic heating to force a full AGCM in order to incorporate the effect of ENSO, rather than relying on the SST. This approach (similar to that of Meehl et al. 2008) circumvents the model uncertainty in diabatic heating response to SST. We modify an existing GCM by adding a relatively small diabatic heating with a vertically idealized structure. The idea is to specify *changes* in the diabatic heating, yet retain the full feedback of the dynamics on the heating in the context of the full model. For example, the rising motion induced by added heating will influence the model's circulation, which in turn can further change the moist and radiative heating fields produced by the models parameterizations. These second-order, or induced, changes are referred to as the “GCM effect” (or coupled dynamical convective response). In reality, cumulus convection (diabatic heating in the model) is coupled with the circulation and can interact with the large-scale dynamics (Watanabe and Jin 2003; Annamalai 2010). Because of the interaction of the diabatic heating with the atmospheric circulation, the specified diabatic heating in this study may not lead to a full understanding of the complexity of the system, but specifying the forced diabatic heating in the model is a first step to understand the relationship between diabatic heating and the monsoon circulation.

To understand under what conditions diabatic heating related to El Niños leads to a dry monsoon, we perform

TABLE 1. El Niño year and monsoon strength in order of its strength.

Year	Niño-3.4 index (JJA)	IMR (JJA)
1997	1.7	Normal
1987	1.5	Dry monsoon
1972	1.1	Dry monsoon
1965	1.0	Dry monsoon
1991	1.0	Weak dry monsoon
1982	0.8	Dry monsoon
1963	0.7	Normal
1994	0.5	Wet monsoon

experiments in which heating/cooling with realistic geographical structure is inserted. The inserted heating is designed so that the total heating, consisting of the inserted heating and the GCM response, matches observed estimates for several ENSO warm events. We include additional heating over the Pacific and Indian Oceans, both together in a full experiment, and separately in sensitivity experiments.

Data used in this study are described in section 2. The characteristics of the observed diabatic heating and wind during strong El Niños are shown in section 3. The experiments of this study are explained in section 4. The responses to the observed forcing for the three strongest El Niño events based on the Niño-3.4 index (1997, 1987, and 1972, see Table 1) are shown in section 5 and 6, respectively.

2. Data

We use several observational and diagnosed quantities including precipitation, winds, streamfunction, velocity potential, and diabatic heating at levels extending from the surface to 100 hPa. The precipitation product is from the National Oceanic and Atmospheric Administration (NOAA) Climate Prediction Center (CPC) Merged Analysis of precipitation (CMAP; Xie and Arkin 1997). The wind data come from the 40-yr European Centre for Medium-Range Weather Forecasts (ECMWF) Re-Analysis (ERA-40) data. The streamfunction, velocity potential, rotational wind, and divergent wind are calculated from the wind data. The diabatic heating data are diagnosed from the ERA-40 data (Chan and Nigam 2009). All datasets are monthly and for analysis we use a summer mean from May through August. This summer mean aligns with the summer simulations (May–August) of this study. The ERA-40 data extend from 1957 to mid-2002 and the Indian Monsoon Rainfall (IMR) data extend from 1871 to 2007. The period that we use here is from 1957 to 2001. The SST data are NOAA optimum interpolation (OI) sea surface temperature (Reynolds

et al. 2002) and the monthly OI SST data cover from 1854 to 2005.

The three-dimensional diabatic heating (Chan and Nigam 2009; Nigam et al. 2000) is diagnosed as a residual in the thermodynamic equation using the analyzed vertical velocity [quasi-diabatic heating (QDB)]. In this study, this diagnosed diabatic heating (Chan and Nigam data), particularly for ENSO, is used to guide our choice of patterns for the inserted forcing in our experiments.

3. Diabatic heating and wind during El Niño

The characteristics of observed mean SST, QDB, and wind anomalies during El Niños are shown as a composite in Fig. 1. [The years chosen for the composite—1963, 1965, 1972, 1982, 1987, 1991, 1994, and 1997—were the years with the largest values of the Niño-3.4 index for summer May–August (MJJA) during the period of 1957–2001. See Table 1.] Both SST and diabatic heating show positive anomalies over the central Pacific (Figs. 1a,b). Weak negative SST anomalies appear over the western Pacific (Fig. 1a), although the negative anomalies of the diabatic heating over the western Pacific (Fig. 1b) have comparable magnitudes to the positive anomalies over the central Pacific.

The anomalous divergent circulation related to ENSO is shown in terms of the velocity potential (χ) and divergent wind at 200 hPa in Fig. 1c. Anomalous upper-level convergent wind and positive velocity potential anomalies over the western Pacific and eastern Indian Ocean imply downward motion, while divergent wind and negative velocity potential anomalies over the central Pacific imply upward motion. The local circulation signal over India itself consisting of positive upper-level velocity potential anomalies and lower-level easterlies over the Arabian Sea is quite weak, although consistent with suppressed convection. This is consistent with the fact that four of the eight years in the composite had near- or above-normal IMR (see Fig. 2), and the average IMR anomaly, while negative, is weak (see Table 2).

Although the anomalous streamfunction and rotational wind at 850 hPa show significant anomalies over the southern Indian Ocean and Pacific in the El Niño composite (in Fig. 1d), weak anomalous anticyclonic circulations extend from the western Pacific to the Indian region. A pair of anomalous cyclonic circulations appears over the central Pacific. These anomalous circulations correspond to the Rossby and Kelvin wave responses in the simple model of Gill (1980). In the composite maps shown here, the influence of El Niño on India does not seem significant, as noted above. However, for those El Niño years in which a significantly weak monsoon (low IMR) occurs, the anomalous atmospheric circulation

becomes important. During the northern summer at 850 hPa, strong climatological southwesterlies over the Arabian Sea provide moisture to India (Fig. 3b). The anomalous anticyclonic circulation near India during El Niño shown in Fig. 1d weakens the southern part of the southwesterly circulation, but strengthens the northern part of the southwesterly. As a consequence, the anomalous anticyclonic circulation influences the Indian monsoon.

For individual warm events Slingo and Annamalai (2000) suggested that a small shift in the locations of sinking motion during ENSO might lead to a modification of the Indian monsoon response. The El Niño composites include both dry and normal (or wet) monsoon years and show only a weak influence on the circulation over India. However, as Slingo and Annamalai (2000) mentioned, among the strongest three events in terms of the Niño-3.4 index (1972, 1987, and 1997), two events (1972 and 1987) show a very distinct velocity potential and convergent wind from the composite and also show a strong negative IMR value (see Fig. 2). The strongest event in terms of Niño-3.4 value is 1997, but the corresponding value of IMR is weak and positive. During the 1972 and 1987 events positive velocity potential and convergent wind anomalies appear over both the western Pacific and the Indian region (Figs. 4a,b). These anomalies imply the extension of the anomalous downward motion over India, consistent with a suppression of monsoon convection and the observed weak monsoon rainfall for both 1972 and 1987. During the 1997 event, while there is strong convergence center over the eastern Indian Ocean and western Pacific, over the Indian region there is relatively weak convergence without the center of convergence (Fig. 4c). So the weak convergence over India in 1997 is more similar to the composite than anomalous convergence in the 1972 and 1987 cases.

The streamfunction and rotational wind fields also show differences in the 1972 and 1987 El Niño events (Fig. 5) compared to the composite (Fig. 1d). The 1987 event has strong anomalous easterlies over the Indian region and Arabian Sea (Fig. 5b), opposing the climatological monsoon flow (Fig. 3b). These anomalies are consistent with the weak monsoon during the 1987 event. During the 1997 case (Fig. 5c), the anomalous anticyclonic circulation is relatively small compared to the 1987 case and the anomalous easterlies over Indian are relatively weak, which is close to the composite (Fig. 1d).

In the 1972 case (Fig. 5a), the anomalous anticyclonic circulation is located slightly off the Indian region. Although the mean velocity potential and divergent winds in Fig. 1c are weak over the Indian region, in 1972 the anomalous velocity potential and divergent winds imply

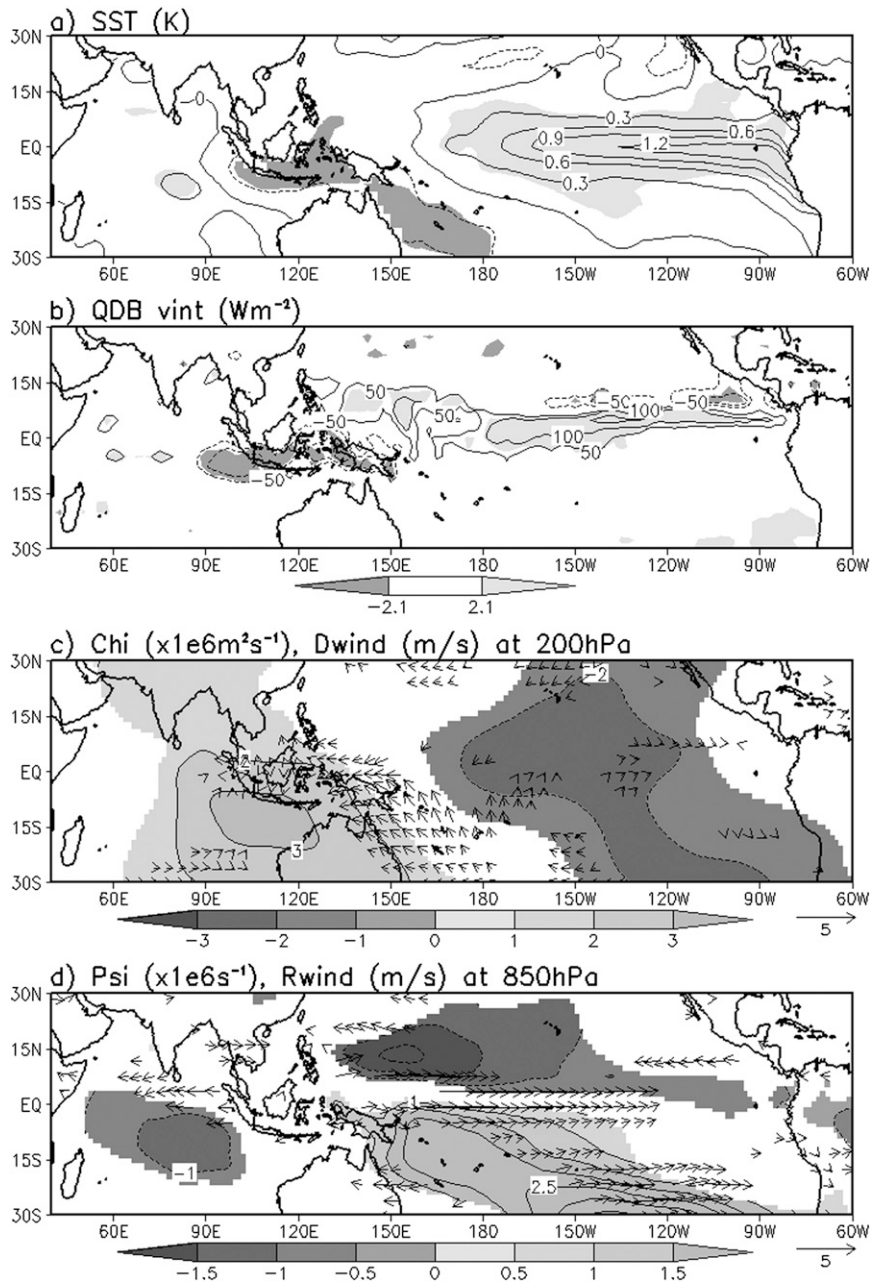


FIG. 1. Observed El Niño composite during its development (May–August seasonal means) see text for explanation of composite. (a) SST anomalies (K). (b) Diabatic heating anomalies vertically integrated from the surface to 100 hPa (W m^{-2}). Shading is 5% significant in (a) and (b). (c) Velocity potential (shading and contour, $\chi \times 10^6 \text{ m}^2 \text{ s}^{-1}$) and divergent wind (vector, m s^{-1}) anomalies at 200 hPa. (d) Streamfunction (shading and contour, $\Psi \times 10^6 \text{ s}^{-1}$) and rotational wind (vector, m s^{-1}) anomalies at 850 hPa. In (c) and (d), only 5% significant values are plotted.

downward motion over the Indian region. It is possible that for the 1972 case the downward motions play a major role in weakening the monsoon without accompanying anomalous easterlies opposing the monsoon flow.

The SST anomalies for the three events are shown in Fig. 6. Over the western (eastern) Pacific negative (positive) anomalies appear in all cases. It is possible that the negative SST anomalies in the western Pacific may be an important direct cause of the anomalous anticyclonic

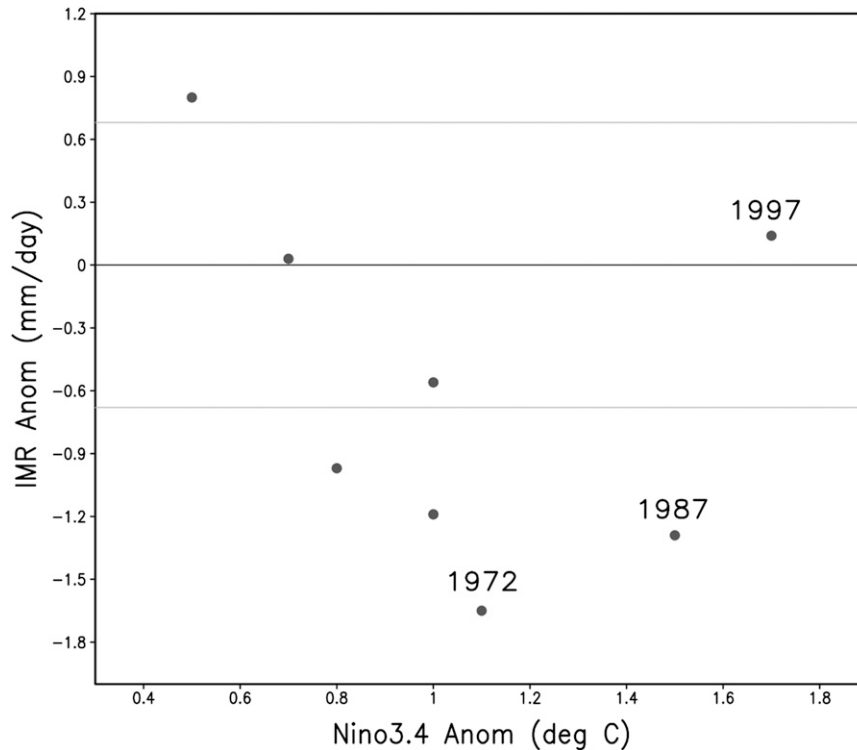


FIG. 2. A scatterplot of the anomalies of the Niño-3.4 index (ordinate) vs the IMR anomalies (abscissa) for 8 El Niño years during summer. The years are 1963, 1965, 1972, 1982, 1987, 1991, 1994, and 1997. The two gray lines indicate ± 1 standard deviation of the IMR.

circulations over the Indian region. In the following section, the response to anomalous diabatic heating over only the western Pacific is examined.

Wide regions of positive SST anomalies over 0.5°C are seen in the Indian Ocean during 1987 and to some extent during 1972, but not during 1997. Yet the corresponding diabatic heating (shown in Fig. 7) indicates substantial and widespread positive anomalies only for 1997. There does not seem to be a direct correspondence between SST and heating anomalies over the Indian Ocean during the period used in this paper. Gadgil et al. (2004) suggest that enhanced convection (negative outgoing longwave radiation anomalies) representing the Indian Ocean dipole (IOD) is closely related to the Indian monsoon and its atmospheric circulation during the 1997/98 event. Ashok et al. (2004) present AGCM experiments in which IOD-related Indian Ocean SST anomalies reduce the influence of ENSO-related SST on the Indian monsoon. However, the IOD-composite SSTs they used are based on months that do not include any of the months shown in Fig. 6. The presence of an Indian Ocean heating anomaly in the absence of an underlying SST anomaly suggests a remote cause. In this paper, the remote cause is not studied but the Indian Ocean warming is emphasized in the experiment section.

The precipitation over India (IMR) for the eight years is listed in Table 2, and three strongest years (1972, 1987, and 1997) are consistent with the maps of anomalous diabatic heating (Fig. 7). The dry monsoon years of 1972 and 1987 have rainfall well below one standard deviation below the mean, whereas the 1997 IMR is slightly above normal but within one standard deviation.

4. Experiments

a. Model

The National Center for Atmospheric Research (NCAR) Community Atmosphere Model, version 3 (CAM3) will be used for the AGCM. The standard

TABLE 2. Seasonal mean (JJAS) of Indian Monsoon Rainfall (mm day^{-1}) (1871–2010).

Mean		7.0	
Std dev		0.68	
El Niño mean		6.42	
Dry monsoon		Normal or wet monsoon	
1965	5.81	1963	7.03
1972	5.35	1991	6.44
1982	6.03	1994	7.80 (wet)
1987	5.71	1997	7.14

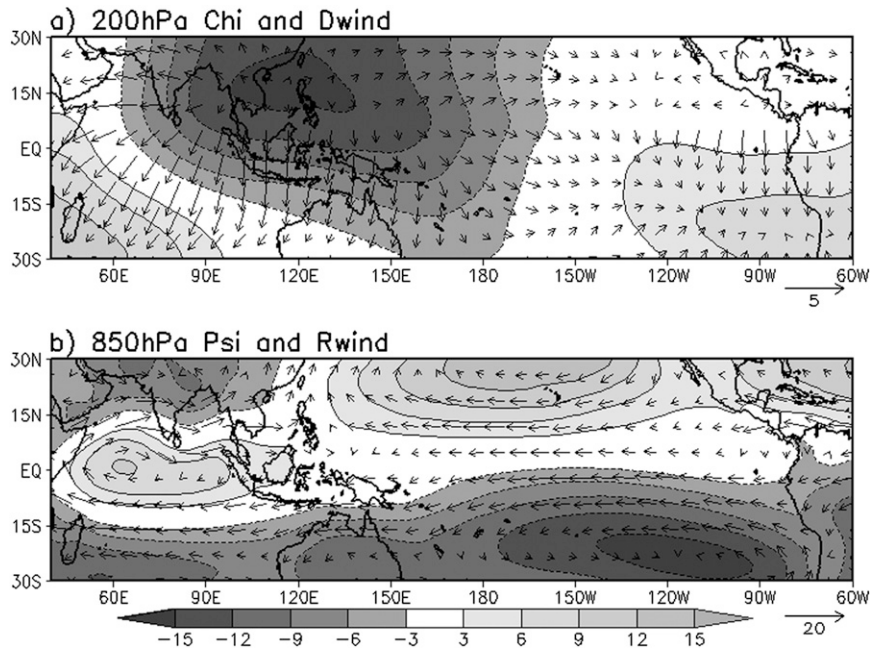


FIG. 3. Climatological summer mean (May–August). (a) Velocity potential (shading and contour, $\chi \times 10^6 \text{ m}^2 \text{ s}^{-1}$) and divergent wind (vector, m s^{-1}) at 200 hPa. (b) Streamfunction (shading and contour, $\Psi \times 10^6 \text{ s}^{-1}$) and rotational wind (vector, m s^{-1}) at 850 hPa.

version, used here, has 26 vertical levels and a 42-wave triangular spectral truncation. The formulation of the physics and dynamics of CAM3 is detailed by Collins et al. (2006). A spectral Eulerian formulation is used to resolve dynamical motions along with a semi-Lagrangian transport scheme for dealing with large-scale transport of water and chemical species. CAM3 also includes the Community Land Model (CLM) version 3.0 for the treatment of land surface energy exchanges. CLM3 is integrated on the same horizontal grid as CAM3.

A slab-ocean model (SOM) will be used for regional air–sea coupling. The ocean model coupled to the AGCM will be a simple thermodynamic slab mixed layer model, which is a part of the NCAR CAM3 modeling system. The depth of the mixed layer is fixed to a climatological annual cycle with a 200-m cap. At each grid point, the AGCM supplies heat flux to the ocean model, and the ocean model returns SST to the AGCM. The SST evolves according to the heat flux given by the AGCM. The coupling will be allowed in only the Indian Ocean and western Pacific (30°S–20°N, 60°–150°E). In the other ocean basins, prescribed climatologically varying monthly SST were used as a boundary condition of the AGCM.

In the tropical central and eastern Pacific, the SST forcing is very strong and we expect that SSTs mainly influence the atmosphere (Lau and Nath 2000, 2003). On

the other hand, for the Indian monsoon region, the experiments of Wu and Kirtman (2005) and Fu and Wang (2002) showed that inclusion of regional air–sea coupling over the Asian monsoon region improved the simulation of the variability of the Asian monsoon rainfall. Wang et al. (2003) and Wang et al. (2005) also stressed the importance of air–sea interaction, particularly of the heat flux exchange for the monsoon region. These studies motivated the inclusion of the regional air–sea interaction in the western Pacific and Indian Ocean. In the extratropics where SSTs are relatively cold, the atmosphere forces the ocean (Lau and Nath 1994). However, in this study, the main interest is the impact of tropical heating on the Indian region, so in order to avoid a complexity in the extratropics the prescribed SST is used.

b. Control run

A control simulation of 21-yr length is run. The control simulation uses prescribed, climatologically varying SSTs outside the Indian and western Pacific oceans, but is coupled to the SOM in the Indian and western Pacific Oceans (30°S–20°N, 60°–150°E); this simulation is called the SOM control run. The prescribed SST has only a climatological annual cycle, so that the effect of interannual variability of the Pacific SST field is not introduced. The SOM control runs will be compared with the forcing experiments in which ENSO-related effects will be introduced through the structure of the added

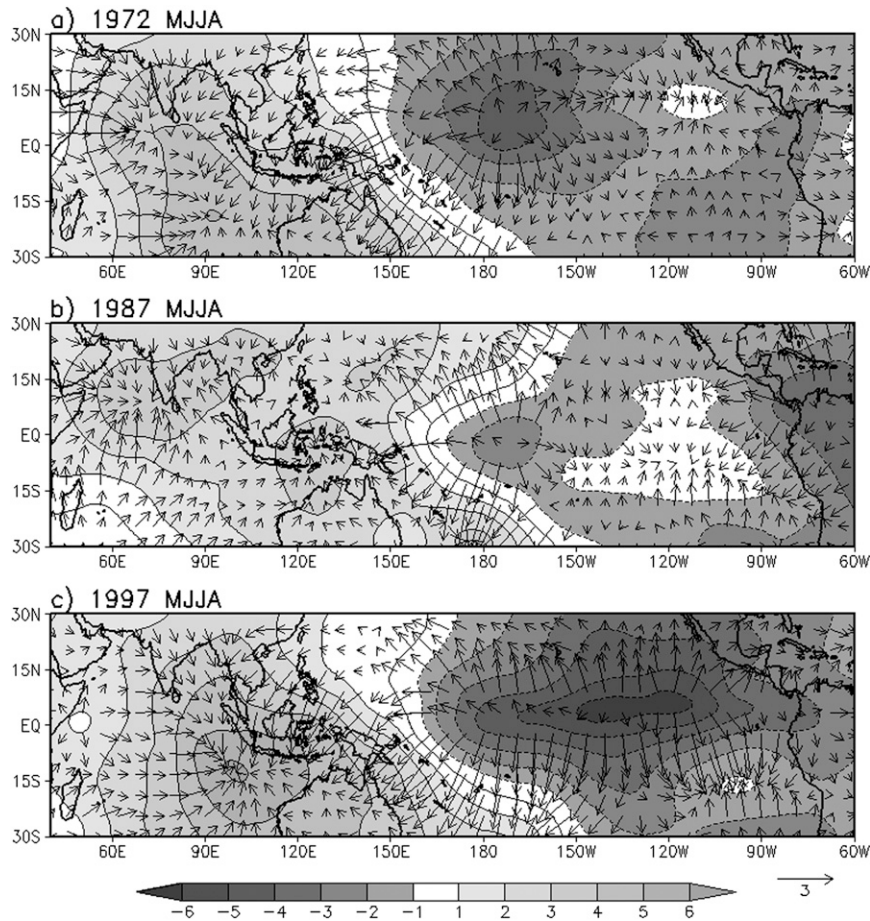


FIG. 4. Anomalous seasonal mean (May–August) velocity potential (shading and contour, $\chi \times 10^6 \text{ m}^2 \text{ s}^{-1}$) and divergent wind (vectors, m s^{-1}) at 200 hPa from ERA-40 reanalysis: (a) 1972 warm event, (b) 1987 warm event, and (c) 1997 warm event.

heating. These forced experiments also incorporate the regional SOM.

c. Forced run

We modified CAM3.0 by adding relatively small diabatic heating fields with an idealized vertical structure. In this method, heating with an idealized vertical profile is added to the temperature tendencies in the GCM. (The heating profile is discussed in the appendix.) The horizontal structure of the added heating was guided by the diagnosed heating anomalies of Chan and Nigam (2009) shown in Fig. 7. In particular, the added heating (shown in Fig. 8) was designed so that the total diabatic heating anomalies (sum of added heating and the CAM generated heating) agrees with Fig. 7. (This involved some trial and error.) For the 1997 case first, three types of forcing are used: 1) forcing A: cooling over the tropical western Pacific and heating over the tropical central/eastern Pacific (Fig. 8c), 2) forcing B: heating

over the tropical Indian Ocean (Fig. 8d), and 3) forcing A plus forcing B (Fig. 8e). In addition, experiments for separating diabatic heating over the central/eastern and western Pacific (from forcing A) are done.

The effect of ENSO-related diabatic heating in the Pacific Ocean is modeled in this paper by adding the diagnosed heating anomalies in this region rather than by specifying the observed SST field for El Niño events in order that the difficulties with the GCM convective parameterizations (incorrect response to SST) may be avoided. However, the case of the 1997 monsoon presents a challenge. The diabatic heating anomaly diagnosed for that year shows substantial heating in the western equatorial Indian Ocean (from 10° – 80°E , as shown in Fig. 7), heating that is larger than in the other two strong El Niño events, and not related in any obvious way to the SST anomaly. Yet that heating anomaly cannot be reproduced either by running the GCM with observed SSTs or by adding the observed Pacific Ocean heating as in this

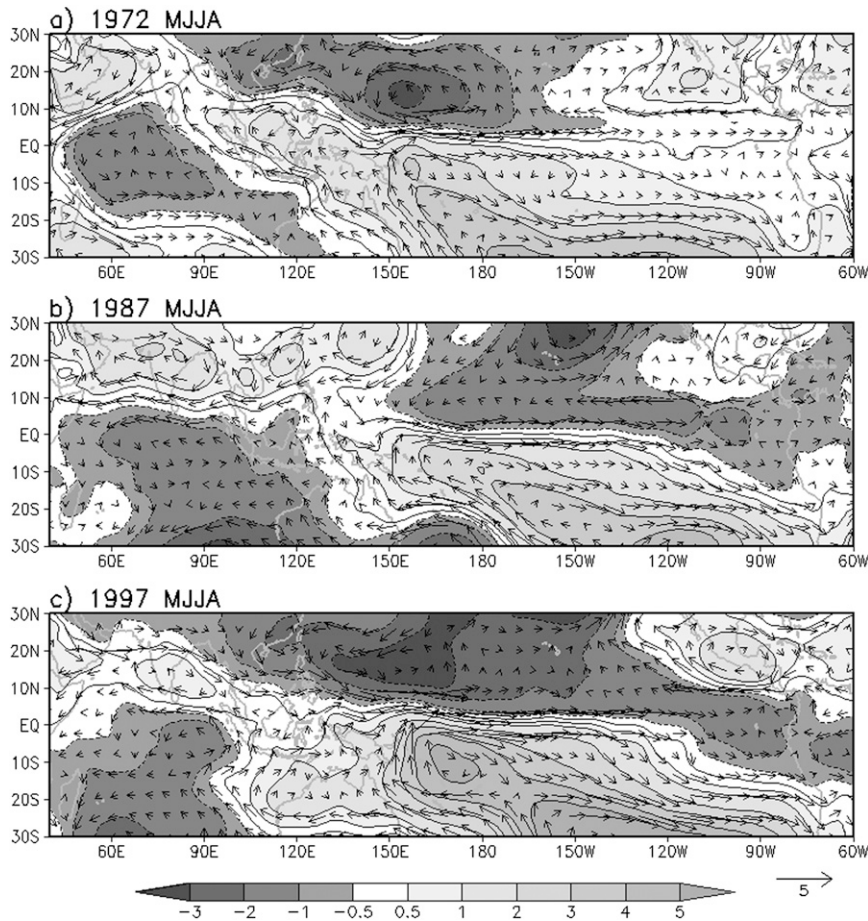


FIG. 5. Anomalous seasonal mean (May–August) streamfunction (shading and contour, $\Psi \times 10^6 \text{ s}^{-1}$) and rotational wind (vector, m s^{-1}) at 850 hPa from ERA-40 reanalysis: (a) 1972 warm event, (b) 1987 warm event, and (c) 1997 warm event.

paper. To understand if this Indian Ocean is relevant to the unusual character of the 1997 Indian monsoon, we have run experiments with the Indian Ocean heating specified (forcing B in Fig. 8d and forcing C in Fig. 8e). While this procedure does not shed light on the cause of the Indian Ocean heating anomaly, it will at least determine whether the anomaly played a role in determining the IMR in 1997.

For each of forced experiments (Fig. 8), 20 seasonal integrations (May–August) were performed using the 20 initial conditions from 1 May from each year of the control simulations. The runs are initialized in May and run through August only because of computer time constraints. Our MJJA average includes the full onset of the monsoon (which can be as early as late May in Sri Lanka), but not the monsoon withdrawal (which occurs in September and even October). We have computed the sensitivity to removing the month of May from the average and it is not large. The 20-run ensemble average

of the May–August seasonal means is compared to the corresponding ensemble seasonal mean from the control simulation. In the analysis, the response to each forcing is calculated as the ensemble time mean difference (forced experiments minus control). In particular, this ensemble procedure is expected to reduce the effect of midlatitude disturbances and in general, internal variability; and we can expect the ensemble mean model response to be dominated by forced waves from tropical heating or cooling. However, there is one caveat to this interpretation of the model results: while the added heating is the same in each of the 20 integrations, the changes in the AGCM's own diabatic heating induced by the additional forcing (called the GCM effect, as explained before), will not necessarily be the same in each of the 20 integrations. The role of internal variability is taken into account in a simple way through the use of the t statistic to assess the difference in all ensemble seasonal means shown.

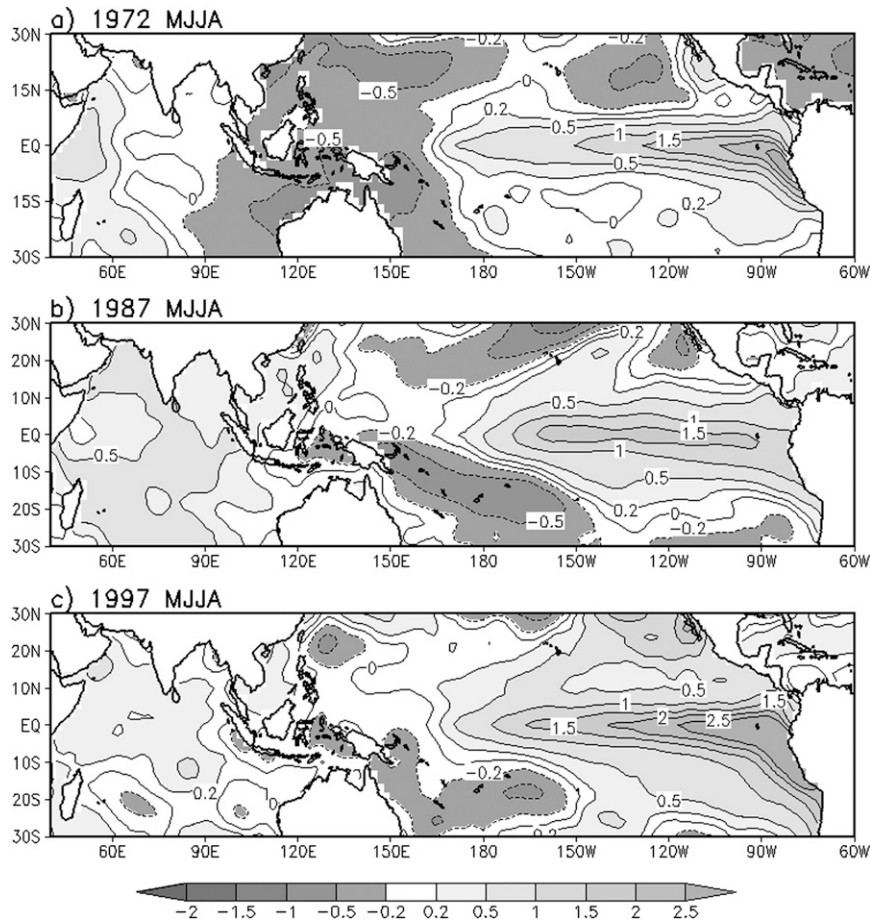


FIG. 6. Anomalous seasonal mean (May–August) SST ($^{\circ}\text{C}$) from observations (see text for details): (a) 1972 warm event, (b) 1987 warm event, and (c) 1997 warm event.

5. 1987/1972 forced experiment

The responses of diabatic heating, the total heating, and precipitation in Figs. 9a–c to the 1987 forcing in Fig. 8a show modest but statistically significant negative anomalies over the Indian region. The experiment with the diagnosed diabatic heating for 1972 summer shows responses (Fig. 10) that are very similar to the 1987 experiment. Recall that the response of the diabatic heating (shown in Fig. 9a) is the additional diabatic heating in the model generated by the coupled dynamical convective response. Over the forcing region in the western Pacific, negative anomalies in the heating response are seen while over the central and eastern Pacific positive heating response anomalies are seen. These anomalies strengthen the total diabatic heating in the model shown in Fig. 9b (cf. Fig. 7b). One manifest thing in terms of this strengthening is the strong negative anomalies near the Sumatra coast. In Fig. 7b, the diagnosed diabatic heating is about $50\text{--}100\text{ W m}^{-2}$, and

while relatively weak forcing is inserted in the model, the model responds strongly near the Sumatra coast.

The responses of the streamfunction and rotational wind at 850 hPa are shown in Figs. 9d and 10d. One pair of anomalous anticyclonic circulations (Rossby response) appears to the west of the negative diabatic heating over the western Pacific. The anticyclonic circulation in the Northern Hemisphere extends toward the Indian region; anomalous easterlies over the Arabian Sea (a part of this anticyclonic circulation) oppose the monsoon flow. However, in Fig. 5a, the observed anticyclonic circulation in 1972 is not strong and does not cover all of India. So the 1972 forced experiment does not simulate the proper anticyclonic circulation, but in terms of velocity potential and convergent winds at 200 hPa (Figs. 9e and 10e) it is consistent with observed convergences in 1972 and 1987 in Figs. 4a,b that show a convergence center over the Indian region. These anomalous easterlies and upper-level convergence implying descending motion both tend to weaken the monsoon. Therefore, anomalous diabatic

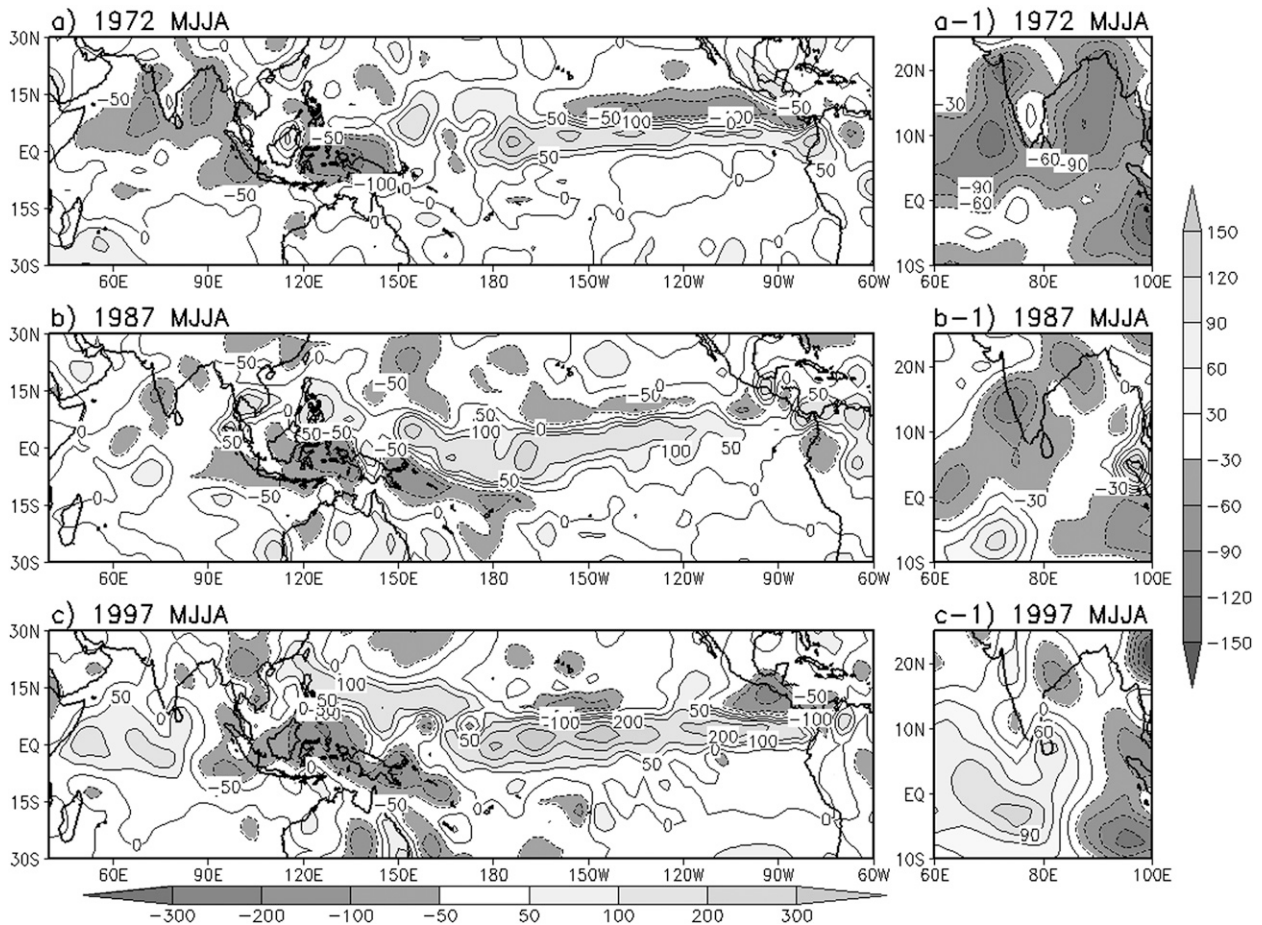


FIG. 7. Vertically integrated anomalous seasonal mean (May–August) diabatic heating (W m^{-2}) estimated from reanalysis (see text for details): (a) 1972 warm event, (b) 1987 warm event, and (c) 1997 warm event. (a-1), (b-1), (c-1) As in (a), (b), (c), but with a smaller contour interval (shown only over the Indian region).

heating related to ENSO (1987 and 1972 forcing) is seen to generate anomalous atmospheric circulation extending toward the Indian region and weakening the Indian monsoon. Because of its weak anticyclonic circulation in 1972, the anomalous downward motion over India may have the dominant impact on weakening the monsoon.

6. 1997 forced experiment

In this section, the forcings in Figs. 8c–e are used to understand the monsoon response to the strong 1997 El Niño. We first consider the experiment in which the added heating consisted of cooling over the western Pacific and heating over the central/eastern Pacific (forcing A in Fig. 8c). The response of the diabatic heating (GCM effect) to this forcing (forcing A) is shown in Fig. 11a. The response is strong over the western Pacific and central/eastern Pacific, which we consider to be the

direct response to the forcing. There are also additional responses such as anomalous cooling in the eastern Pacific, which is also seen in the observed diabatic heating (Fig. 11, top). The forcing and response are combined to form the total diabatic heating in the model. Although the positive response over the equatorial eastern Pacific is relatively weak in Fig. 11a, the total diabatic heating (Fig. 11e) has comparable magnitude to the observed diabatic heating (Fig. 11, top) because the inserted heating has almost the same magnitude as the observed heating. In terms of the Indian monsoon, the Pacific forcing (forcing A) simulates negative anomalies of the diabatic heating (Fig. 11a) and negative precipitation (Fig. 12a) over India. This result is consistent with that of the 1987 experiment.

The anomalous diabatic heating in Fig. 11 (top) is strong and well developed over the central Pacific, but the observations in 1997 show no diabatic heating anomalies and normal precipitation over India [Fig. 11 (top) and

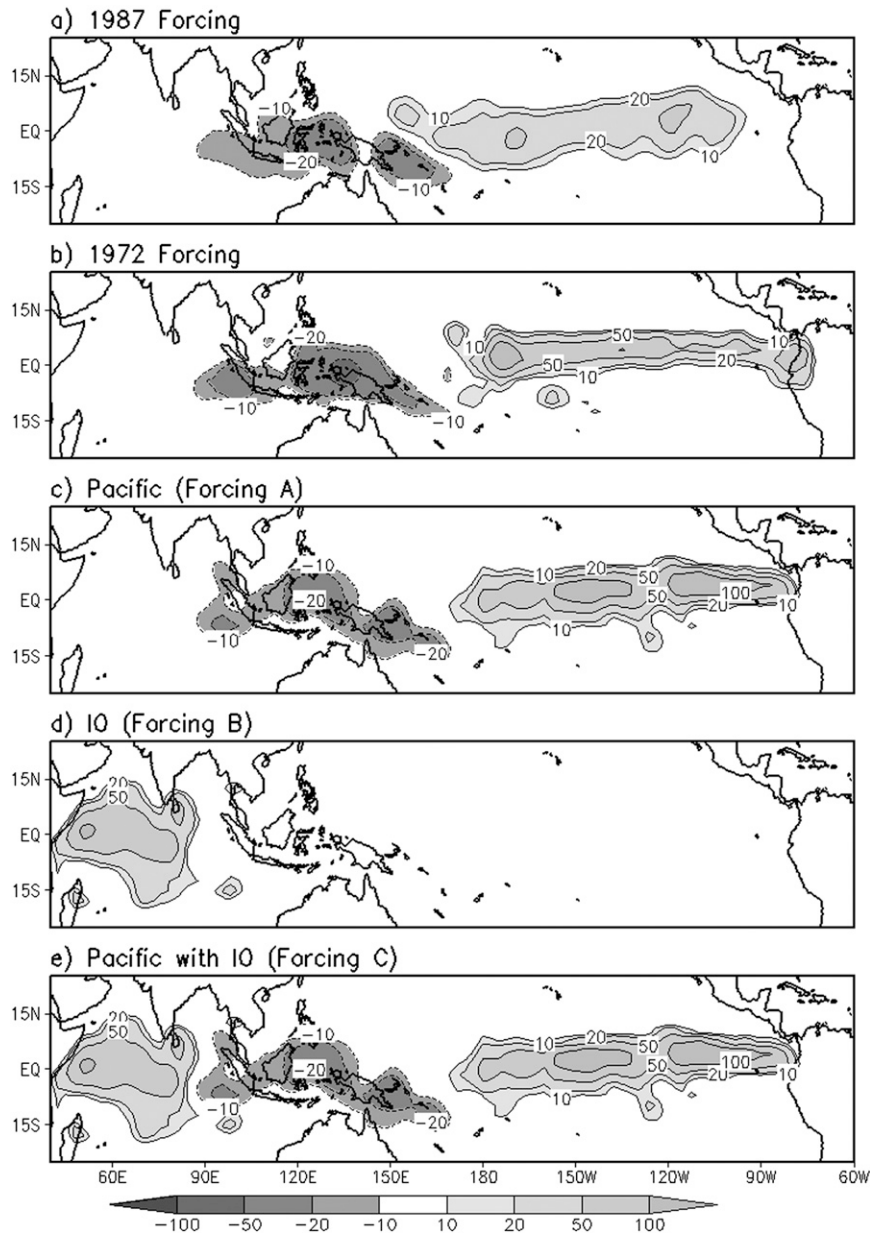


FIG. 8. Idealized heating (forcing) added for each experiment: (a) 1987 forcing, (b) Pacific forcing only for 1997 experiment (forcing A), (c) the Indian Ocean forcing only (forcing B), and (d) Pacific and Indian Ocean forcing (forcing C). Each forcing is vertically integrated; units are (W m^{-2}).

Table 2]. In the model, heating over the Indian Ocean is added to the Pacific heating fields in the second experiment of the 1997/98 event (Forcing C in Fig. 8e). [A similar 1997 experiment with the Indian Ocean warming has also been carried out by Ashok et al. (2004) and Su et al. (2001), but in an AGCM with SST forcing.] The inclusion of the Indian Ocean added heating leads to the absence of any significant anomalies of diabatic heating over India (Fig. 11d), and the response of precipitation

also does not show significant anomalies over India (Fig. 12c). This is consistent with the observed diabatic heating (Fig. 11, top) and the modest value of the Indian Monsoon Rainfall (Table 2), which imply a normal monsoon. The total diabatic heating over the equatorial Indian Ocean, western Pacific, and central/eastern Pacific in the model (Fig. 11h) also have comparable magnitudes with the observed ones. Therefore, the Indian Ocean heating seems to be one crucial factor contributing

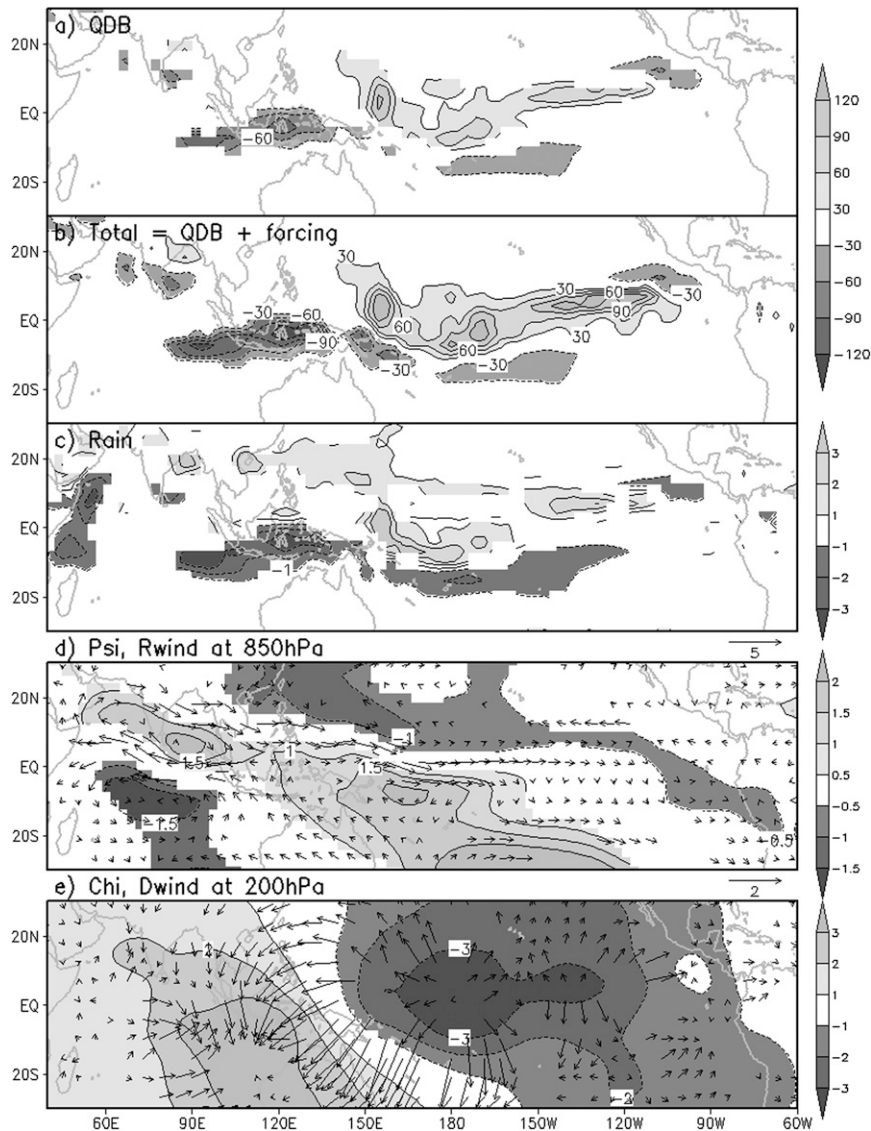


FIG. 9. Results of 1987 experiment (seasonal mean, May–August): (a) anomalous GCM heating response (vertically integrated, W m^{-2}), (b) total heating (GCM response plus forcing, W m^{-2}), (c) precipitation (mm day^{-1}), (d) streamfunction (shading and contour, $\Psi \times 10^6 \text{ s}^{-1}$) and rotational wind (vector, m s^{-1}) at 850 hPa, and (e) velocity potential (shading and contour, $\chi \times 10^6 \text{ m}^2 \text{ s}^{-1}$) and divergent wind (vectors, m s^{-1}) at 200 hPa. Only 5% significant values are plotted.

to the lack of the Indian monsoon drought in 1997. However, this is only a first step; since we have not been able to reproduce the Indian Ocean heating as a remote response to Pacific SSTs, its origin is not clear. But we have established that it seems to be relevant in explaining the 1997 monsoon. Su et al. (2001) also found in their simplified AGCM that warm SST over the Indian Ocean contributes to the local enhanced rainfall, more so even than the strong El Niño warming in the eastern equatorial Pacific. In addition, Annamalai and Liu (2005) argued

that the Indian Ocean should be included to understand the ENSO–monsoon linkage in terms of prediction of rainfall.

In this study, the focus is forced responses by anomalous diabatic heating and the anomalous Indian Ocean heating is used as forcing. However, the cause of the Indian Ocean heating (precipitation anomalies) is also an important issue because it is possible that the monsoon circulation induced by external forcing can modify the diabatic heating substantially. Experiments B and C

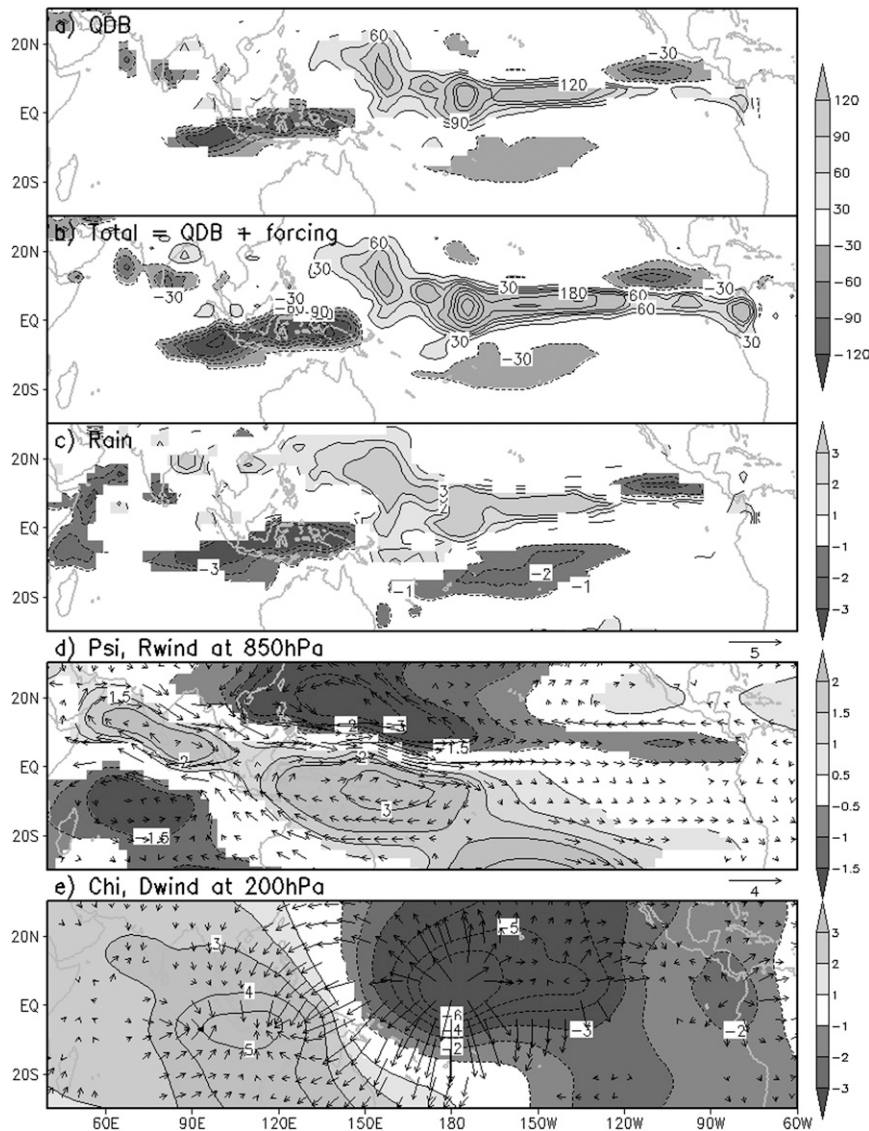


FIG. 10. As in Fig. 9, but for 1972.

show only that there is a connection between Indian Ocean heating and the monsoon rainfall.

It is also of interest to examine the response of the atmospheric circulation to the Pacific and Indian Ocean forcings. The Pacific forcing without the Indian Ocean warming simulates a large anticyclonic circulation extending toward India and the western Indian Ocean as shown in Fig. 13a. The response of rotational wind shows strong easterlies extending from the equatorial western Pacific across the western Indian Ocean, thus weakening the climatological monsoon flow in Fig. 3b. On the other hand, when the Indian Ocean warming is added to the Pacific forcing, the easterlies to the south of India do not extend to the western Indian Ocean (Fig. 13d). The

weakened and limited easterly anomalies and anticyclonic circulation are similar to the observed streamfunction and wind anomalies shown in Fig. 5c.

To further understand the role of the Indian Ocean (IO) warming, the IO warming alone (forcing B in Fig. 8d) is inserted in the model. In terms of rotational wind, weak westerlies to the west of the heating (over the equatorial Indian Ocean to the west of India) are shown in Fig. 13b and the streamfunction at 1000 hPa shows one weak cyclonic center of circulation to the west of India (Fig. 13b-1). The westerlies to the west of India (Fig. 13b) oppose the easterly anomalies forced by the Pacific forcing over the equatorial Indian Ocean (a part of the anticyclonic circulation seen in Fig. 13a).

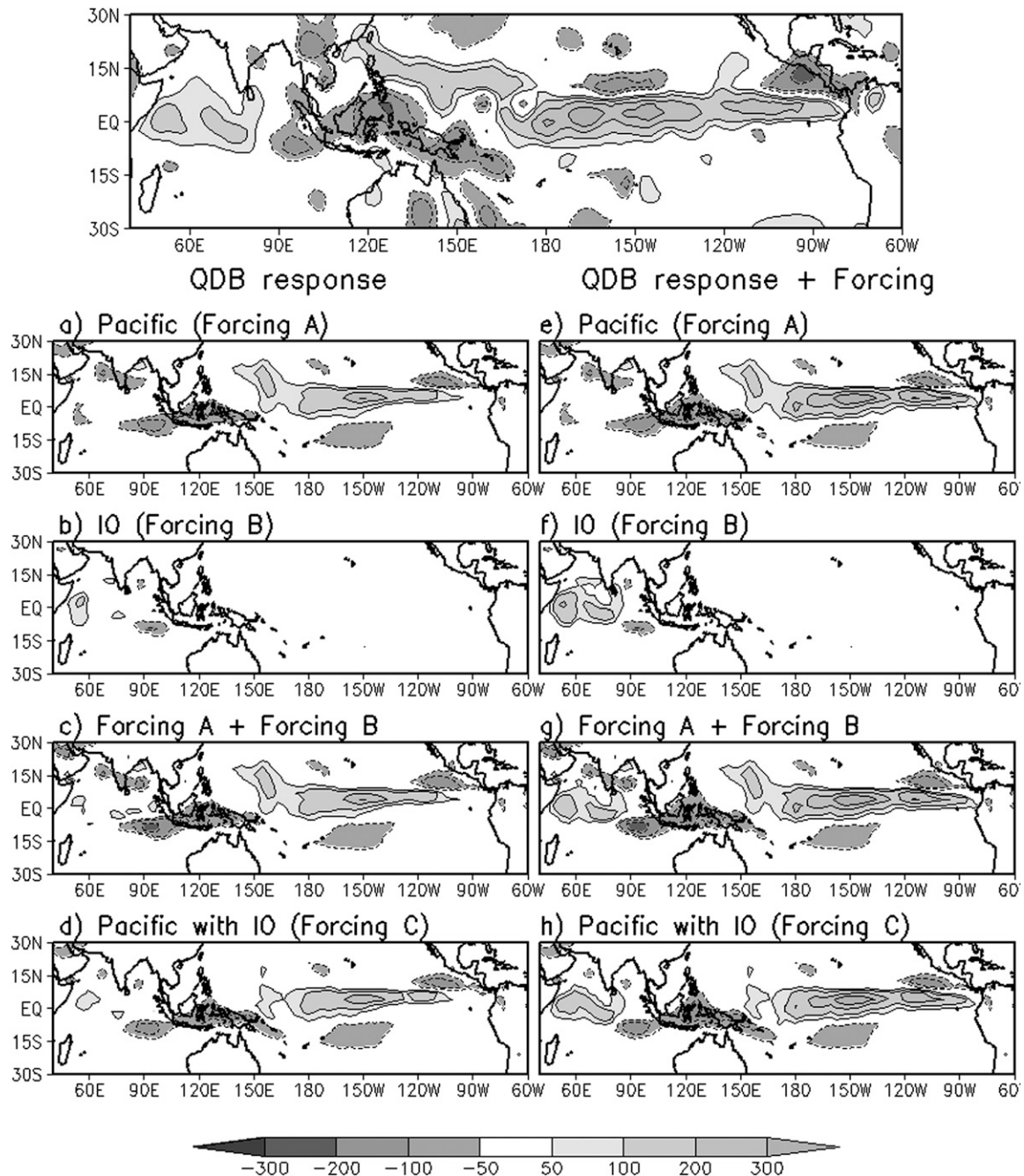


FIG. 11. (top) Anomalous vertically integrated diabatic heating (W m^{-2} ; May–August mean) for 1997 estimated from ERA-40. The vertically integrated diabatic heating response (W m^{-2}) to each forcing: (a) Pacific forcing (forcing A), (b) IO warming (forcing B), (c) linear combination of the two responses (forcing A and forcing B), and (d) Pacific forcing with IO forcing (forcing C). The sum of diabatic heating response and forcing (vertically integrated) for each forcing: (e) Pacific forcing (forcing A), (f) IO warming (forcing B), (g) linear combination of the two responses (forcing A and forcing B), and (h) Pacific forcing with IO forcing (forcing C). Only 5% significant values are plotted in (a)–(h).

We also investigate the linear combination of the response to the Pacific and IO forcing. The diabatic heating response to forcings A and B are linearly added is shown in Fig. 11c, with the corresponding total in Fig. 11g. The

sum of the streamfunction and rotational wind at 850 hPa to the two forcings (Fig. 13c) shows weakened anticyclonic circulation over the Indian region compared to the Pacific-only forcing case (Fig. 13a), but the magnitude of

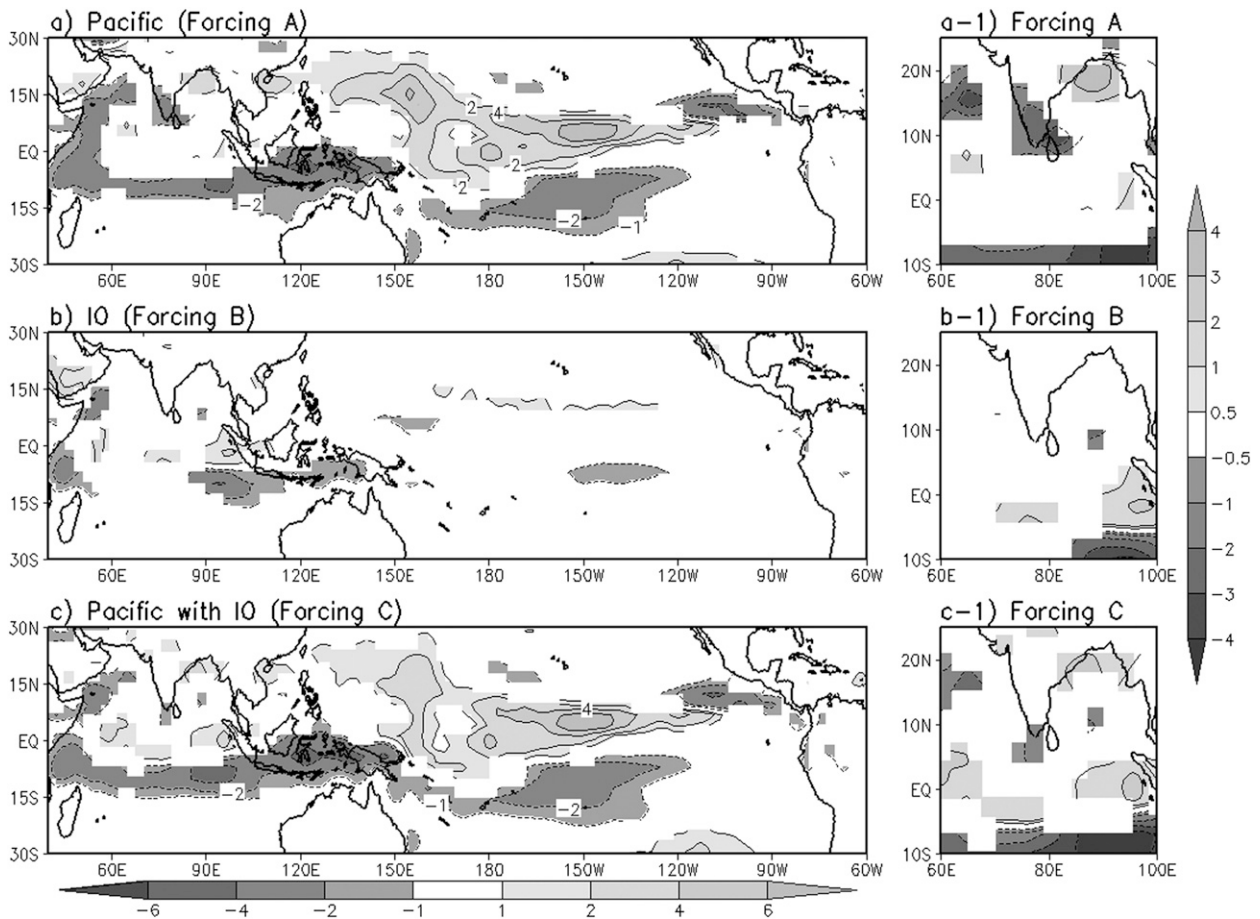


FIG. 12. Anomalous seasonal mean (May–August) precipitation response (mm day^{-1}) in the three 1997 experiments: (a) Pacific forcing (forcing A), (b) IO warming (forcing B), and (c) Pacific forcing with IO forcing (forcing C). Only 5% significant values are plotted. (a-1), (b-1), (c-1) As in (a), (b), (c), but with a smaller contour interval (shown only over the Indian region).

streamfunction over the Indian Ocean (Fig. 13c) is stronger than in the response to both Pacific and IO forcings (Fig. 13d). There is clearly some nonlinear compensation taking a place between the responses to IO and Pacific added heating.

The velocity potential and divergent winds at 200 hPa also show the changes in the anomalous divergent circulation due to adding the IO warming (Fig. 14). When the forcing is over only the Pacific, convergent wind with positive velocity potential appears over the western Pacific and Indian region, which weakens the monsoon convection by anomalous downward motion (Fig. 14a). However, when the IO warming is added, this convergent wind and positive velocity potential (Fig. 14d) are not centered in the Indian region; instead divergent wind and negative velocity potential appear over the western Indian Ocean implying anomalous ascending motion. When only the IO warming is inserted (Fig. 14b), strong divergent wind and negative velocity potential appear

over the western Indian Ocean. The linear combination of the Pacific and IO warming (Fig. 14c) shows features that are similar to the response of the Pacific forcing with the IO warming (Fig. 14d). The observed velocity potential and divergent wind during the 1997 event (Fig. 4c) show similar features as well. Therefore, the anomalous ascending motion by the IO warming weakens the anomalous descending motion over the Indian region, leading to a lack of strong monsoon anomalies.

Additional experiments are done in order to measure the effects of the heating over the western and eastern Pacific separately (see forcing A in Fig. 8c). Figures 15 and 16 show the results of the western Pacific (WP) and the central Pacific (CP) forcing, respectively. The WP forcing alone induces the negative anomalies of diabatic heating and precipitation near the Indian region and anomalous anticyclonic circulation at 850 hPa in Fig. 15, which is related to a weak Indian monsoon. However, anomalous diabatic heating and precipitation are not

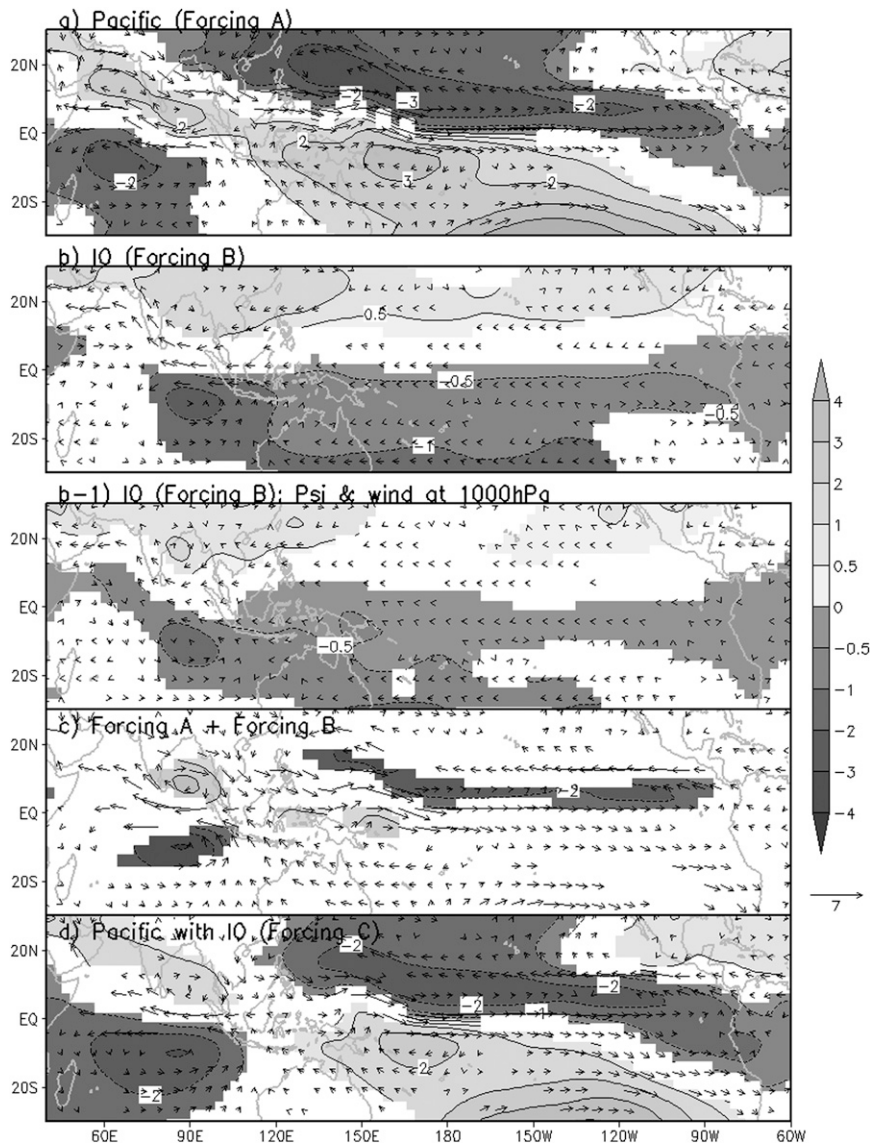


FIG. 13. Seasonal mean (May–August) anomalies of streamfunction (shading and contour, $\Psi \times 10^6 \text{ s}^{-1}$) and rotational wind response (vector, m s^{-1}) at 850 hPa to three 1997 experiments: (a) Pacific forcing (forcing A), (b) IO warming (forcing B), (b-1) IO warming [streamfunction and rotational wind at 1000 hPa only for (b-1)], (c) linear combination of two response (forcing A and forcing B), and (d) Pacific forcing with IO forcing (forcing C). Only 5% significant values are plotted.

strong as the results of the combined Pacific forcing (forcing A) in Figs. 11a and 12a. At 200 hPa the anomalous divergent field related to downward motion also does not appear in this experiment (Fig. 15e). On the other hand, the CP forcing alone is more similar to the results of the combined Pacific forcing. The anomalously negative diabatic heating and precipitation over the Indian region in Figs. 16a,c show comparable strengths compared with the results of the combined Pacific forcing. The divergent field at 200 hPa and streamfunction at

850 hPa are also more similar to the results of the combined Pacific forcing than the WP forcing alone. Thus, considering only the Pacific forcing for 1997 case, the CP forcing has a stronger influence on the Indian monsoon than the WP forcing.

In this section, the 1997 experiment with the Pacific-only forcing shows results similar to those of the 1987 and 1972 experiments seen in the previous section. However, in the diabatic heating diagnosed from ERA-40, 1997 has a strong IO warm component comparable to the

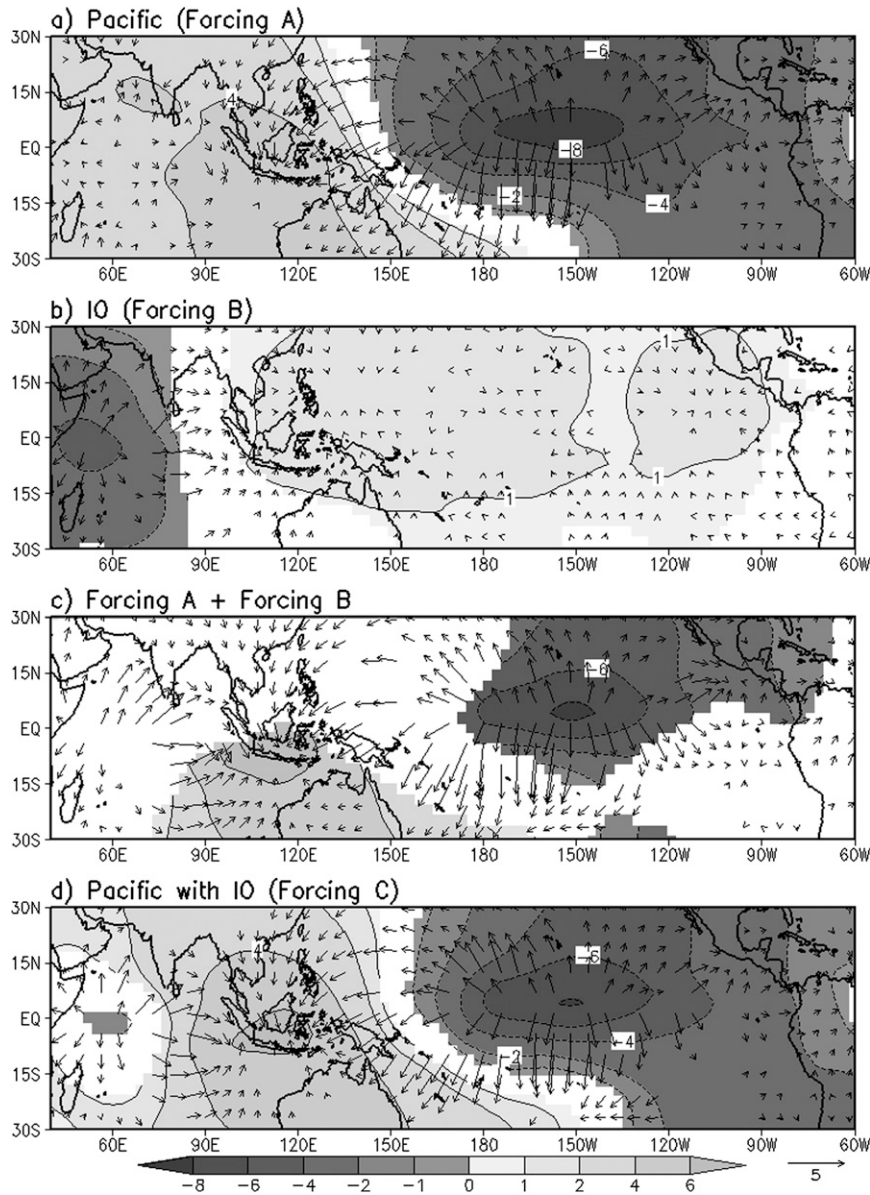


FIG. 14. Seasonal mean (May–August) anomalies of velocity potential (shading and contour, $\chi \times 10^6 \text{ m}^2 \text{ s}^{-1}$) and divergent wind response (vector, m s^{-1}) to three 1997 experiments: (a) Pacific forcing (forcing A), (b) IO warming (forcing B), (c) linear combination of two response (forcing A and forcing B), and (d) Pacific forcing with IO forcing (forcing C). Only 5% significant values are plotted.

anomalous diabatic heating over the western Pacific and eastern Pacific. By adding the IO warming to the Pacific additional heating we find that the GCM response of diabatic heating indicates a normal monsoon. The streamfunction and velocity potential also show circulation consistent with the normal monsoon. In terms of the atmospheric response, therefore, it is concluded that the Indian Ocean warming plays a role in modifying the influence of ENSO on the Indian monsoon.

7. Conclusions

To understand the relationship between ENSO and the Indian summer monsoon, the atmospheric response to the tropical diabatic heating is studied in a GCM. Instead of traditional approaches, such as inserting SST forcing in an AGCM, or specifying diabatic heating in a simple idealized GCM, we modify an existing GCM by adding a relatively small diabatic heating with an

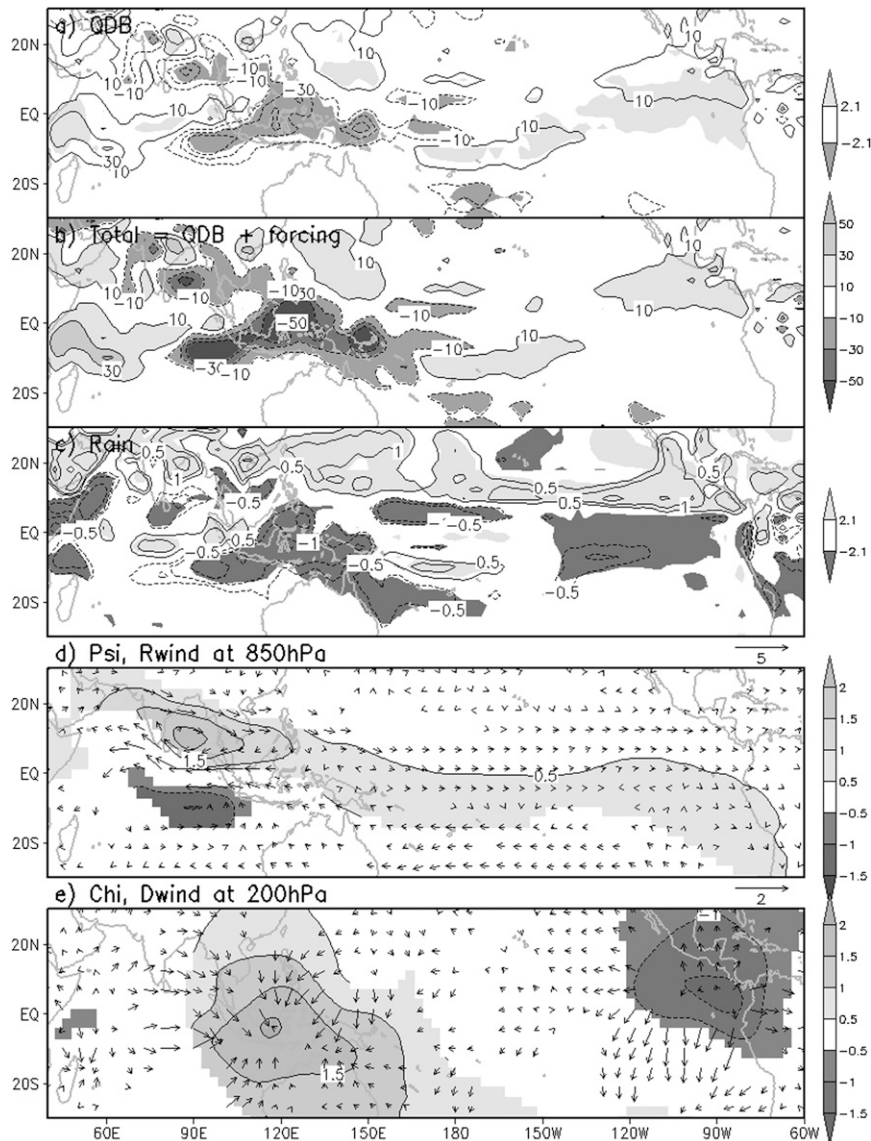


FIG. 15. Results of WP experiment (seasonal mean, May–August): (a) anomalous GCM heating response (vertically integrated, W m^{-2}), (b) total heating (GCM response plus forcing, W m^{-2}), (c) precipitation (mm day^{-1}), (d) streamfunction (shading and contour, $\Psi \times 10^6 \text{ s}^{-1}$) and rotational wind (vector, m s^{-1}) at 850 hPa, and (e) velocity potential (shading and contour, $\chi \times 10^6 \text{ m}^2 \text{ s}^{-1}$) and divergent wind (vectors, m s^{-1}) at 200 hPa. In (d) and (e), only 5% significant values are plotted.

idealized vertical structure. In this method, the anomalous circulation by added heating/cooling will influence the model's circulation, which in turn further changes diabatic heating fields (additional diabatic heating) as the coupled dynamical-convective response (GCM effect).

Although warm ENSO events lead to a characteristic change in the tropical circulation, each ENSO event has a different detailed spatial pattern. Diagnosed diabatic heating data show that the 1997 event was accompanied

by a relatively strong heating anomaly over the Indian Ocean. This anomaly is not manifest during other very strong El Niño events such as 1972 and 1987. The anomalous Indian Ocean heating cannot be reproduced either by running the GCM with observed SSTs, or by adding the observed Pacific Ocean heating as in this paper. So in this study, the experiments were designed to understand how those two distinct diabatic heatings produce as forcing, the atmospheric circulation differently and how they influence the Indian monsoon differently.

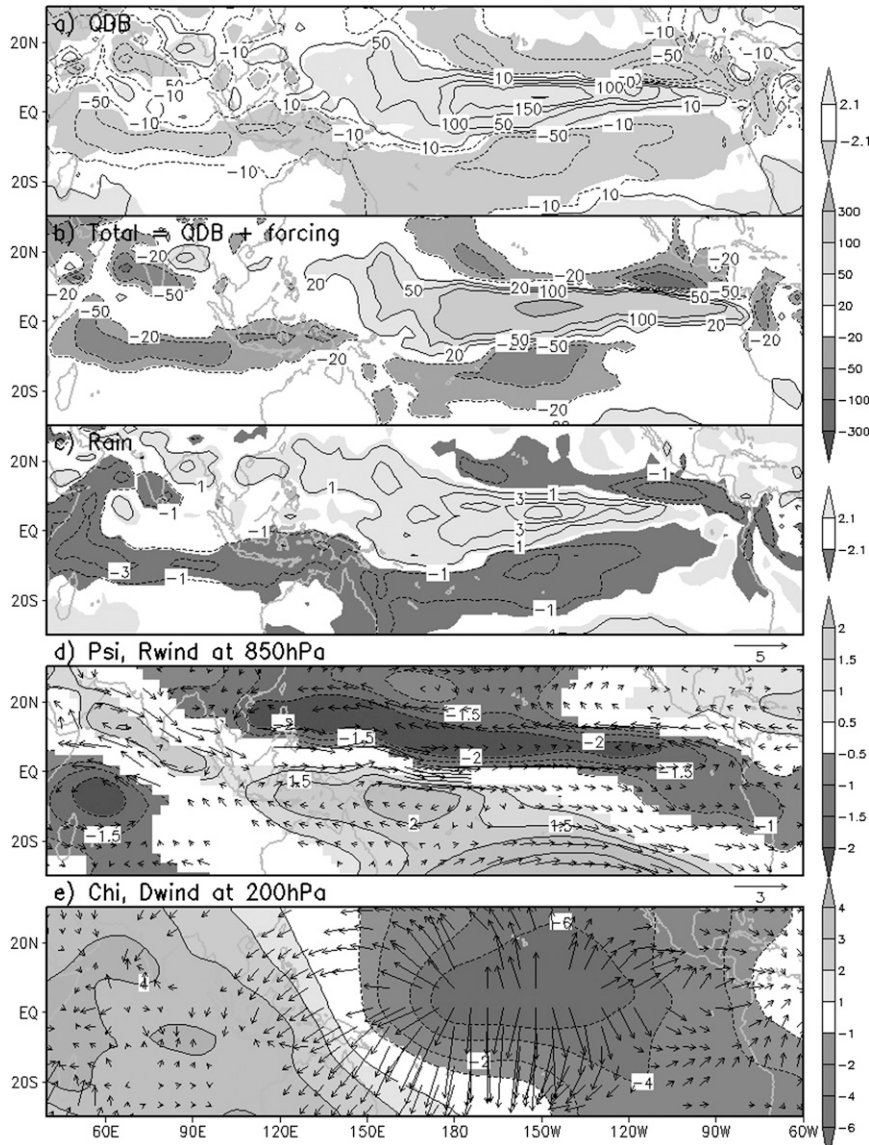


FIG. 16. As in Fig. 15, but for the CP experiment.

The Pacific diabatic heating is used in the 1987, 1972, and 1997 experiments. Negative diabatic heating over the western Pacific and positive diabatic heating over the central/eastern Pacific (consistent with estimates from reanalysis for those years) induces a downward motion branch over the extended Indian region and this implies weakening of monsoon convection. Moreover, an anticyclonic circulation (Rossby response) to the west of the western Pacific cooling is also manifest. Anomalous easterlies as a part of this anticyclonic circulation are opposed to the climatological monsoon flow and tend to weaken the monsoon. Pillai and Annamalai (2012) identified anticyclonic circulation related to these easterlies as the precursor signal over South

Asia that advects dry air to South Asia and leads to a dry monsoon.

For the experiments for the 1997 case show that the effect of the central Pacific heating dominates that of the western Pacific cooling. In the 1997 experiment, the additional Indian Ocean heating leads to a compensation of this anticyclonic circulation. The Indian Ocean heating, thus, tends to suppress the response to the Pacific heating, leading to a normal monsoon circulation.

In this study, the anomalous large-scale atmospheric circulation induced by tropical heating is shown to be a reasonable explanation of the relationship between El Niño and the Indian monsoon. However, for the 1972

TABLE A1. Standard values (h_k) of midlevel pressure (Pa) for hybrid coordinate system for CAM3.

Level K	Pressure	Level K	Pressure
1	354.5	14	22 651.3
2	739.9	15	26 648.1
3	1396.7	16	31 350.1
4	2394.5	17	36 881.8
5	3723.0	18	43 389.5
6	5311.5	19	51 045.5
7	7005.9	20	60 052.4
8	8543.9	21	69 679.6
9	10 051.5	22	78 770.2
10	11 825.0	23	86 716.1
11	13 911.5	24	92 964.9
12	16 366.2	25	97 055.5
13	19 254.0	26	99 255.6

TABLE A2. Coefficients of A_m and B_m , $M = 2$; harmonic coefficients correspond to heating of Eq. (A2).

	$m = 1$	$m = 2$
A_m	-0.0418	-0.0392
B_m	-0.6917	-0.3230

warm event the anomalous anticyclonic circulation was not strong enough to explain the observed weakening of the monsoon. Only the downward branch induced by the anomalous divergent circulation extending westward into India was consistent with a dry monsoon. It is possible that other important factors such as the boreal summer intraseasonal oscillation (Krishnamurthy and Shukla 2000) or land-atmospheric interaction could have been important during 1972.

It should be pointed out that while our results suggest the importance of the Indian Ocean heating for the 1997 monsoon circulation, they do not constitute a complete explanation, since the Indian Ocean heating was given a priori. In reality, this heating is also a product of the large-scale circulation as well as possibly remote SSTs.

Acknowledgments. We are grateful for discussions with Dr. J. Shukla. This work was supported by the National Science Foundation (Grants ATM-0830062 and ATM-0830068), the National Oceanic and Atmospheric Administration (Grant NA09 OAR4310058), the National Aeronautics and Space Administration (Grant NNX09AN50G) and the Office of Science (BER) of the U.S. Department of Energy (Grant DE-FG02-07ER64473). Computing support from the Climate Simulation Laboratory of the National Center of Atmospheric Research is also acknowledged.

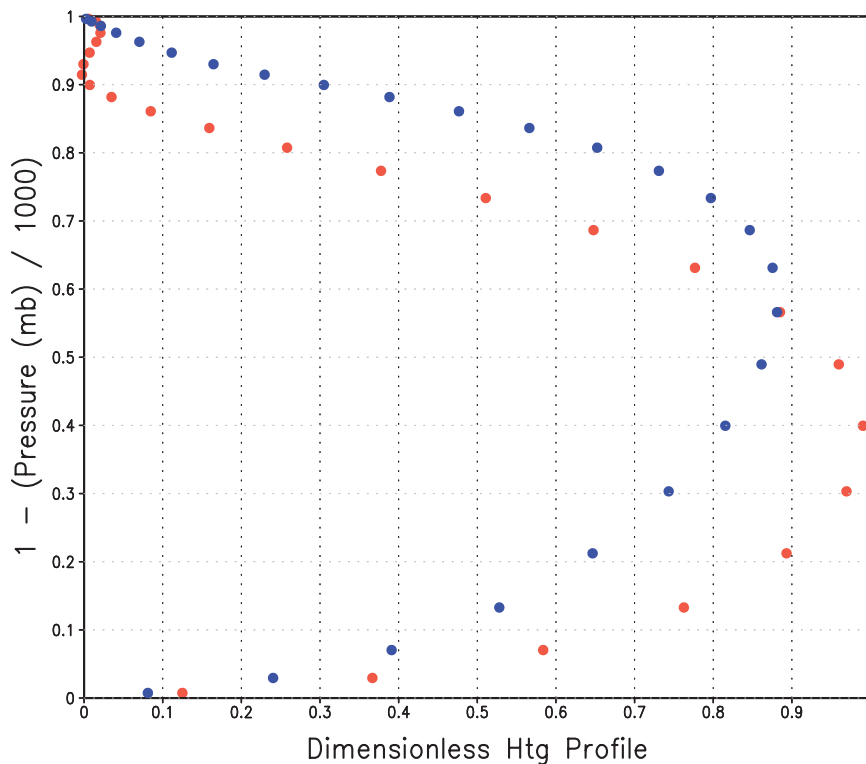


FIG. A1. Heating profiles derived by harmonic approximation. See the appendix for details. Blue dots are from Eq. (A1) and red dots are from Eq. (A2).

APPENDIX

Vertical Profile

Two types of idealized vertical structure are approximated and then they are compared with the observed vertical structure to decide which one gives a better approximation to the observed structure. The vertical structure of the perturbation is generated as follows. The hybrid vertical coordinates are specified as input and the corresponding midlayer pressures are calculated from these assuming a fixed surface pressure of $p_0 = 1000$ hPa. We use a standard set of $K = 26$ levels, with midlayer pressure values h_k as given in the Table A1.

For a profile to become very small at the bottom and top of the model, we use this approximation:

$$\hat{F}_k \approx \sum_{m=1}^M \left[A_m \cos\left(2\pi \frac{mk}{K}\right) + B_m \sin\left(2\pi \frac{mk}{K}\right) \right]. \quad (\text{A1})$$

The values of A_m and B_m are given in Table A2 using $m = 2$. Equation (A1) is implemented in the CAM3 subroutine (dynamics and physics coupling module), in which the full temperature tendency is available in gridpoint configuration. The resulting profile is given by the blue dots in Fig. A1.

To achieve a somewhat shallower profile, we modify the formula in Eq. (1):

$$F_k = \sin\left(\pi \frac{h_k}{p_0}\right) - 0.3 \sin\left(2\pi \frac{h_k}{p_0}\right) - 0.1 \sin\left(4\pi \frac{h_k}{p_0}\right). \quad (\text{A2})$$

An extended heating is defined as above, and Fig. A1 shows this heating profile as the red dots.

To compare the two profiles with observed diabatic heating, the vertical structure of anomalous diabatic heating fields obtained from ERA-40 data by Chan and Nigam (2009) is shown for El Niño and La Niña events in Fig. A2. Two types of the vertical structures are shown: those for a single grid point (2.5°S, 132°E, solid lines with closed circles for El Niño) and one for spatially averaged values (5°S–2°N, 120°–140°E, dashed lines for El Niño). In Fig. A1, the shallow vertical profiles show a maximum at 600 mb and the deep profiles show the maximum at about 450 mb. ERA-40 diabatic heating for both El Niño and La Niña shows the maximum below 500 mb, although each event has a somewhat different vertical structure. In all the experiments in this paper, the shallower profile (red dots in Fig. A1) is used for the vertical structure.

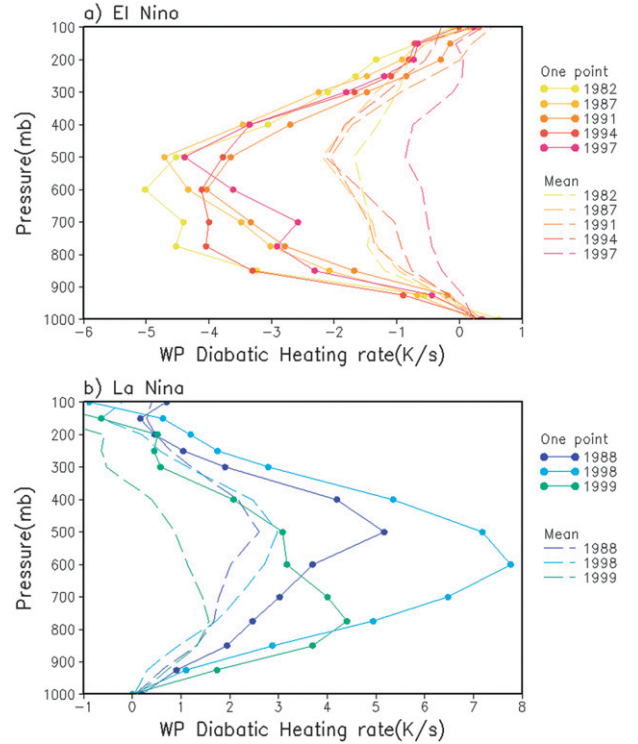


FIG. A2. The vertical structure of ERA-40 diabatic heating rate (K s^{-1}). (a) For El Niño events (1982, 1987, 1991, 1994, and 1997). The solid lines with closed circles are at 2.5°S, 132°E. The dashed lines are averaged from 5°S–2°N to 120°–140°E. (b) For La Niña events (1988, 1998, and 1999). The solid lines with closed circles are at 2.5°S, 137°E for 1988 and at 2.5°S, 100°E for 1998 and 1999. For 1988 the dashed lines are averaged from 5°S–2°N to 130°–140°E and for 1998 and 1999 they are averaged from 5°S–2°N to 95°–105°E.

Note that since we have assumed the surface pressure equal to p_0 . The coordinate in Fig. A1 should really be the model coordinate; the correspondence with pressure is only valid if the true surface pressure is close to p_0 , typically over the ocean.

REFERENCES

- Annamalai, H., 2010: Moist dynamical linkage between the equatorial Indian Ocean and the South Asian monsoon trough. *J. Atmos. Sci.*, **67**, 589–610.
- , and P. Liu, 2005: Response of the Asian monsoon to changes in El Niño properties. *Quart. J. Roy. Meteor. Soc.*, **131**, 805–831.
- Ashok, K., Z. Guan, N. H. Saji, and T. Yamagata, 2004: Individual and combined influences of ENSO and the Indian Ocean dipole on the Indian summer monsoon. *J. Climate*, **17**, 3141–3155.
- Chan, S. C., and S. Nigam, 2009: Residual diagnosis of diabatic heating from ERA-40 and NCEP reanalyses: Intercomparisons with TRMM. *J. Climate*, **22**, 414–428.
- Charney, J. G., and J. Shukla, 1981: Predictability of monsoons. *Monsoon Dynamics*, J. Lighthill and R. P. Pearce, Eds., Cambridge University Press, 99–110.

- Collins, W. D., and Coauthors, 2006: The formulation and atmospheric simulation of the Community Atmosphere Model version 3 (CAM3). *J. Climate*, **19**, 2144–2161.
- Fu, X., and B. Wang, 2002: Impacts of air–sea coupling on the simulation of mean Asian summer monsoon in the ECHAM4 model. *Mon. Wea. Rev.*, **130**, 2889–2904.
- Gadgil, S., P. N. Vinayachandra, P. A. Francis, and S. Gadgil, 2004: Extremes of the Indian summer monsoon rainfall, ENSO and equatorial Indian Ocean oscillation. *Geophys. Res. Lett.*, **31**, L12213, doi:10.1029/2004GL019733.
- Gill, A. E., 1980: Some simple solutions for heat-induced tropical circulation. *Quart. J. Roy. Meteor. Soc.*, **106**, 447–462.
- Jin, F., and B. J. Hoskins, 1995: The direct response to tropical heating a baroclinic atmosphere. *J. Atmos. Sci.*, **52**, 307–319.
- Ju, J., and J. M. Slingo, 1995: The Asian summer monsoon and ENSO. *Quart. J. Roy. Meteor. Soc.*, **121**, 1133–1168.
- Kirtman, B. P., and J. Shukla, 2000: Influence of the Indian summer monsoon on ENSO. *Quart. J. Roy. Meteor. Soc.*, **126**, 213–239.
- Kripalani, R. H., and A. Kulkarni, 1997: Climate impacts of El Niño/La Niña on the Indian monsoon: A new perspective. *Weather*, **52**, 39–46.
- Krishnamurthy, V., and J. Shukla, 2000: Intraseasonal and interannual variability of rainfall over India. *J. Climate*, **13**, 4366–4377.
- Kucharski, F., A. Baracco, J. H. Yoo, and F. Molteni, 2007: Low-frequency variability of the Indian monsoon–ENSO relationship and the tropical Atlantic: The “weakening” of the 1980s and 1990s. *J. Climate*, **20**, 4255–4266.
- Kumar, K. K., B. Rajagopalan, and M. A. Cane, 1999: On the weakening relationship between the Indian monsoon and ENSO. *Science*, **284**, 2156–2159.
- Lau, N. C., and M. J. Nath, 1994: A modeling study of the relative roles of tropical and extratropical SST anomalies in the variability of the global atmosphere–ocean system. *J. Climate*, **7**, 1184–1207.
- , and —, 2000: Impact of ENSO on the variability of the Asian–Australian monsoons as simulated in GCM experiments. *J. Climate*, **13**, 4287–4309.
- , and —, 2003: Atmosphere–ocean variations in the Indo-Pacific sector during ENSO episodes. *J. Climate*, **16**, 3–20.
- Lin, H., 2009: Global extratropical response to diabatic heating variability of the Asian summer monsoon. *J. Atmos. Sci.*, **66**, 2697–2713.
- Meehl, G. A., J. M. Arblaster, and G. Branstator, 2008: A coupled air–sea response mechanism to solar forcing in the Pacific region. *J. Climate*, **21**, 2883–2897.
- Nigam, S., C. Chung, and E. DeWeaver, 2000: ENSO diabatic heating in ECMWF and NCEP reanalyses, and NCAR CCM3 simulation. *J. Climate*, **13**, 3152–3171.
- Palmer, T. N., C. Brankovic, P. Viterbo, and M. J. Miller, 1992: Modeling interannual variations of summer monsoons. *J. Climate*, **5**, 399–417.
- Pillai, P. A., and H. Annamalai, 2012: Moist dynamics of severe monsoons over South Asia: Role of the tropical SST. *J. Atmos. Sci.*, **69**, 97–115.
- Reynolds, R. W., N. A. Rayner, T. M. Smith, D. C. Stokes, and W. Wang, 2002: An improved in situ and satellite SST analysis for climate. *J. Climate*, **15**, 1609–1625.
- Sahai, A. K., A. M. Grimm, V. Satyan, and G. B. Pant, 2003: Long-lead prediction of Indian summer monsoon rainfall from global SST evolution. *Climate Dyn.*, **20**, 855–863.
- Shukla, J., and D. A. Paolino, 1983: The Southern Oscillation and long-range forecasting of the summer monsoon rainfall over India. *Mon. Wea. Rev.*, **111**, 1830–1837.
- Slingo, J. M., and H. Annamalai, 2000: 1997: The El Niño of the century and the response of the Indian summer monsoon. *Mon. Wea. Rev.*, **128**, 1778–1797.
- Straus, M. D., and V. Krishnamurthy, 2007: The preferred structure of the interannual Indian monsoon variability. *Pure Appl. Geophys.*, **164**, 1717–1732.
- Su, H., J. D. Neelin, and C. Chou, 2001: Tropical teleconnection and local response to SST anomalies during 1997–1998 El Niño. *J. Geophys. Res.*, **106** (D17), 20 025–20 044.
- Wang, B., R. Wu, and X. Fu, 2000: Pacific–East Asian teleconnection: How does ENSO affect East Asian climate? *J. Climate*, **13**, 1517–1536.
- , —, and T. Li, 2003: Atmosphere–warm ocean interaction and its impacts on Asian–Australian monsoon variation. *J. Climate*, **16**, 1195–1211.
- , Q. Ding, X. Fu, I.-S. Kang, K. Jin, and J. Shukla, 2005: Fundamental challenge in simulation and prediction of summer monsoon rainfall. *Geophys. Res. Lett.*, **32**, L15711, doi:10.1029/2005GL022734.
- Watanabe, M., and F. Jin, 2003: A moist linear baroclinic model: Coupled dynamical–convective response to El Niño. *J. Climate*, **16**, 1121–1139.
- Wu, R., and B. Kirtman, 2005: Roles of Indian and Pacific Ocean air–sea coupling in tropical atmospheric variability. *Climate Dyn.*, **25**, 155–170.
- Xie, P., and P. A. Arkin, 1997: Global precipitation: A 17-year monthly analysis based on gauge observations, satellite estimates, and numerical model outputs. *Bull. Amer. Meteor. Soc.*, **78**, 2539–2558.